tvst

DOI: 10.1167/tvst.4.4.1

Article

Intrasurgical Human Retinal Imaging With Manual Instrument Tracking Using a Microscope-Integrated Spectral-Domain Optical Coherence Tomography Device

Paul Hahn[1], Oscar Carrasco-Zevallos[2], David Cunefare[2], Justin Migacz[2], Sina Farsiu[1,2], Joseph A. Izatt[2], and Cynthia A. Toth[1,2]

[1] Department of Ophthalmology, Duke University Medical Center, Durham, NC, USA
[2] Department of Biomedical Engineering, Duke University, Durham, NC, USA

Correspondence: Cynthia A. Toth, MD; Box 3802, DUMC, Durham, NC 27710, USA.
e-mail: cynthia.toth@duke.edu

Received: 12 January 2015
Accepted: 28 March 2015
Published: 1 July 2015

Keywords: spectral-domain optical coherence tomography; OCT; microscope-mounted; microscope-integrated; intraoperative; vitreoretinal surgery; human imaging; real-time; tracking

Citation: Hahn P, Carrasco-Zevallos O, Cunefare D, et al. Intrasurgical human retinal imaging with manual instrument tracking using a microscope-integrated spectral-domain optical coherence tomography device. Tran Vis Sci Tech. 2015;4(4):1, doi:10.1167/tvst.4.4.1

Purpose: To characterize the first in-human intraoperative imaging using a custom prototype spectral-domain microscope-integrated optical coherence tomography (MIOCT) device during vitreoretinal surgery with instruments in the eye.

Methods: Under institutional review board approval for a prospective intraoperative study, MIOCT images were obtained at surgical pauses with instruments held static in the vitreous cavity and then concurrently with surgical maneuvers. Postoperatively, MIOCT images obtained at surgical pauses were compared with images obtained with a high-resolution handheld spectral-domain OCT (HHOCT) system with objective endpoints, including acquisition of images acceptable for analysis and identification of predefined macular morphologic or pathologic features.

Results: Human MIOCT images were successfully obtained before incision and during pauses in surgical maneuvers. MIOCT imaging confirmed preoperative diagnoses, such as epiretinal membrane, full-thickness macular hole, and vitreomacular traction and demonstrated successful achievement of surgical goals. MIOCT and HHOCT images obtained at surgical pauses in two cohorts of five patients were comparable with greater than or equal to 80% correlation in 80% of patients. Real-time video-imaging concurrent with surgical manipulations enabled, for the first time using this device, visualization of dynamic instrument-retina interaction with targeted OCT tracking.

Conclusion: MIOCT is successful for imaging at surgical pauses and for real-time image guidance with implementation of targeted OCT tracking. Even faster acquisition speeds are currently being developed with incorporation of a swept-source MIOCT engine. Further refinements and investigations will be directed toward continued integration for real-time volumetric imaging of surgical maneuvers.

Translational Relevance: Ongoing development of seamless MIOCT systems will likely transform surgical visualization, approaches, and decision-making.

Introduction

Following the revolutionary impact of optical coherence tomography (OCT) imaging in the clinical evaluation of retinal diseases, there has been growing interest in use of this imaging technology in the operating room. The commercial availability of spectral-domain OCT (SDOCT) imaging using a portable handheld system has allowed retinal surgeons to obtain images of retinal morphology at pauses during surgical maneuvers. There have been increasing numbers of reports of SDOCT imaging with a portable handheld system to reveal intraoperative changes in retinal morphology during vitreoretinal surgery.[1–10] In addition to handheld positioning, these portable SDOCT systems have also been stabilized using a microscope-mount (Bioptigen, Inc., Research Triangle Park, NC) or a separate stand-mount (Optovue, Inc., Fremont, CA) to obtain images. Regardless of the method to support the portable systems, their intraoperative imaging can only be obtained by halting surgery, removing all instruments from the eye, stabilizing the eye, and moving the microscope away from the surgical

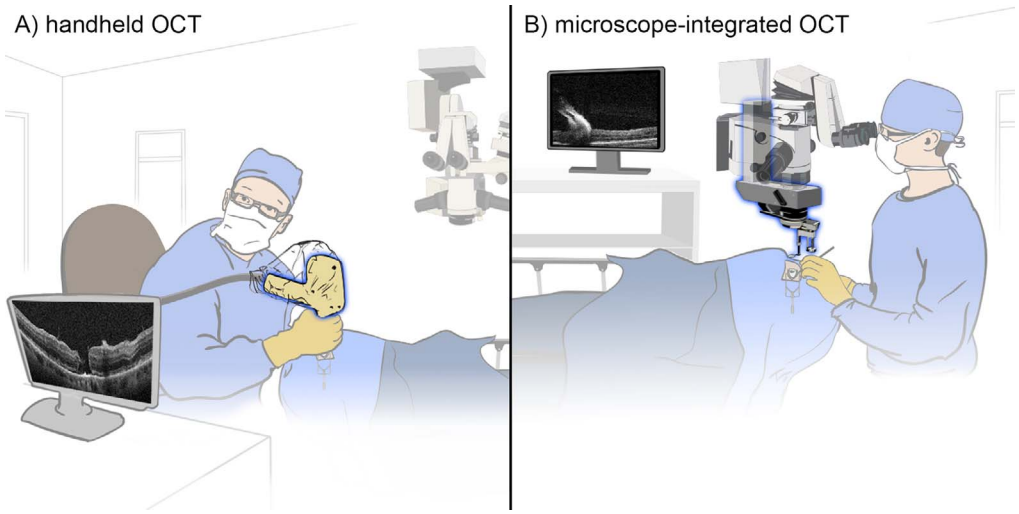

Figure 1. Illustration comparing the use of HHOCT and MIOCT. HHOCT (A) requires a full pause in surgery, removal of the microscope away from the surgical field, and placement of a portable OCT scanner with a sterile wrap over the eye to obtain images viewed on a separate computer screen. In contrast, MIOCT (B) is integrated into the surgical microscope, enabling OCT acquisition simultaneous with ongoing surgical manipulations. Instrument-retina interactions can only be imaged with MIOCT.

field in order to position the scanner over the eye (Fig. 1A). Imaging with portable SDOCT scanners is therefore limited by their inability to image the retina with instruments in the eye or concurrently with surgical maneuvers in real time.

To address this limitation, our group has developed a novel research prototype microscope-integrated SDOCT (MIOCT) device, which enables OCT acquisition simultaneous with surgical maneuvers (Fig. 1B).[1,11–14] Several groups have also reported recent development of other SDOCT systems integrated within the operating microscope toward simultaneous imaging and surgery.[15–17] We have previously described the technical design of the MIOCT scanner, which is based on folding of the optical OCT path into the full beam path of the operating microscope to enable high-resolution SDOCT imaging simultaneous with surgical viewing.[1,11,12,14,18,19] In this report, we present results of MIOCT image acquisition first at pauses in surgery with instruments safely positioned in the mid-vitreous cavity and then concurrently with surgical maneuvers, and we identify future important requirements for progression toward seamless intrasurgical MIOCT imaging.

Methods

MIOCT Design

As we have previously described, a high-resolution MIOCT prototype device was developed to interface optically and mechanically with an ophthalmic operating microscope (Leica Microsystems, Heerbrugg, Switzerland).[11] Briefly, a dichroic mirror allows folding of the MIOCT optical path into the surgical microscope above the objective lens to permit simultaneous imaging during surgical manipulations without altering the surgeon's view. At this insertion point, the OCT beam was expanded to the ideal width for high-resolution, diffraction-limited imaging of the retina. This prototype microscope-integrated scanner was coupled with a Bioptigen SDOCT imaging engine with a center wavelength of 865 nm and a spectrometer equipped to acquire images at a rate of 20,000 A-scans per second. The lateral resolution was 15 μm, and the field of view was 10 × 10 mm. The axial resolution was 5 μm and the depth range was 1.55 mm.

Human Imaging

The Duke Health System institutional review board approved (IRB) this research protocol, which was also in accordance with the Declaration of Helsinki and all applicable Health Insurance Portability and Accountability Act regulations. A Data and Safety Monitoring Committee "plus" (which includes participants outside the institution) reviewed and approved the protocol and study progress. Informed consent was obtained per protocol from all patients participating in this study after discussing the nature and possible consequences of the study. The study is posted at clinicaltrials.gov #NCT01588041. Eligible patients were those undergoing retinal surgery (with CAT or PH), with the

exclusion of eyes with corneal or media opacities that would potentially interfere with OCT imaging.

Prior to the initiation of surgery, the MIOCT scanner was mounted onto the Leica surgical microscope. Optical and power cables were coursed along the microscope arm and ceiling to a computer workstation positioned to drive the MIOCT scanner and to receive the OCT image output. A dedicated member of the research team was assigned to operate the computer workstation. Optical power emitted from the OCT system was measured before and after all MIOCT imaging to ensure patient safety as per the IRB protocol.

MIOCT imaging was performed by first positioning the MIOCT-equipped microscope to center the surgical view over the pupil. The MIOCT scanner was engineered to scan the OCT beam concentrically with the viewing axis of the microscope, and MIOCT alignment was obtained as the surgeon oriented the globe at the start of surgery for optimal focus at the surgeon's standard view. Once the surgeon was in focus for retinal work, the research team fine-tuned the alignment and focus of the OCT beam and the reference arm position.

All imaging was performed in the operating room on eyes undergoing macular surgery performed by two surgeons (CAT and PH). Standard three-port 25-gauge pars plana vitrectomy was performed. As is the standard surgical practice pattern by these surgeons, indocyanine green (ICG)-assisted peeling of the internal limiting membrane (ILM) was performed for all cases of epiretinal membrane (ERM), vitreomacular traction (VMT), and full-thickness macular hole (FTMH). Images were obtained with the patient supine on the surgical bed using both MIOCT and HHOCT, both of which were performed under sterile conditions with the patient fully draped and the lid speculum in place. Initial imaging with HHOCT was performed prior to incision as previously described.[1] Initial MIOCT imaging was performed following placement of surgical cannulas and optimal alignment of the surgeon's view of the macula, as visualized through the surgical microscope with a Binocular Indirect Ocular Microscope (BIOM; Oculus Inc., Port St. Lucie, FL) wide-angle noncontact viewing system and an endoilluminating light source.

We previously reported planned stepwise translation of MIOCT imaging toward integrated human imaging in a prospective study consisting of three sequential stages (Supplemental Table 1).[1] In stage 1, we successfully used the MIOCT system to obtain images at pauses in surgical manipulations with all instruments removed from the eye and compared these images with those obtained with a handheld SDOCT (HHOCT) device.[1] In this study, we proceeded with Stage 2 and 3. In Stage 2, intraoperative MIOCT imaging was obtained at the start of surgery and at pauses following surgical manipulations, with the instruments stationary in the midvitreous cavity as further proof of concept that this device can obtain images during surgery. In Stage 3, MIOCT imaging was obtained at the above time points as well as concurrently with macular surgical manipulations. Intraoperative imaging was obtained through either the BIOM or a plano-concave contact lens at the surgeon's discretion. MIOCT and HHOCT images were also captured at the completion of macular surgical maneuvers but prior to fluid-air exchange and cannula removal. Total OCT imaging time, including both MIOCT and HHOCT, was limited to 30 minutes per surgical case.

A real-time manual tracking system was developed and incorporated into the MIOCT during the course of this study to assist imaging of dynamic surgical maneuvers for Stage 3 imaging. Special purpose tracking software allowed a technician to dynamically trace the desired point of OCT imaging within the surgical field of view using a mouse pointer overlaid on the video feed from the surgical camera. The lateral position of the mouse cursor over the surgical camera frame was then calculated and converted into corresponding scanning mirror offsets used to relocate the OCT scan to the desired position. Prior to imaging, the tracking system was calibrated to ensure that the mouse cursor position correlated with OCT scan location on the en face view provided by a surgical video camera. This tracking system allowed live, dynamic relocation of the OCT scan position through real-time repositioning of a mouse cursor to any area of interest.

Image Acquisition and Post Processing

MIOCT images were acquired with an 8-mm B-scan length with 1000 A-scans/B-scan. Volumes were acquired over an 8×8–mm area when applicable. Live preview images were obtained in real time with adjustment of brightness and contrast as needed but without any post processing modifications. All data analysis was performed on these unprocessed, live images. For review, images were post processed with a previously published sparsity-based simultaneous denoising and interpolation (SBSDI) method.[20] The SBSDI algorithm is based on the compressive sensing paradigm and uses a previously collected dataset of low-quality and corresponding high-quality images to

Table. Surgical Cases and Intraoperative Stage 2 MIOCT Imaging Results

Case	Preoperative Pathology	Surgical Procedure	Surgery Uncomplicated?	Acceptable Imaging?[a]	% Correlation MIOCT-to-HHOCT[b]
1	ERM	25G PPV/MP (ICG)	Yes	Yes	100
2	VMT	25G PPV/MP (ICG)	Yes	Yes	100
3	ERM	25G PPV/MP (ICG)	Yes	Yes	100
4	ERM	25G PPV/MP (ICG)	Yes	Yes	60
5	ERM	25G PPV/MP (ICG)	Yes	Yes	100
6	ERM	25G PPV/MP (ICG)	Yes	Yes	20
7	FTMH	25G PPV/MP (ICG)	Yes	Yes	100
8	ERM	25G PPV/MP (ICG)	Yes	Yes	80
9	FTMH	25G PPV/MP (ICG)	Yes	Yes	100
10	ERM	25G PPV/MP (ICG)	Yes	Yes	100

[a] Defined as ability to visualize inner retinal surface and RPE interface in at least one MIOCT image.

[b] Defined as number of identifiable elements, (1) macular hole, (2) epiretinal membrane, (3) retinal edema, schisis or cystoid structures, (4) subretinal fluid or retinal detachment, and (5) central retinal thickness from inner retina to RPE, in MIOCT compared with HHOCT images.

learn the inherent image degradation model in an imaging system. SBSDI software is freely available online and has been previously used for reliable denoising of OCT images in human and murine eyes without increasing image blur.[20,21] For this paper, the training set was acquired using the same system as in this study and used seven pairs of low- and high-quality images. The high-quality images were obtained by registering and averaging 14 to 18 images from the same position. All parameters were the same as used in the original SBSDI paper[20] except that for MIOCT denoising, we used a dictionary patch size of 6×4 pixels.

Data Analysis

MIOCT and HHOCT images obtained during Stage 2 from matched time points without any post processing were scored by two graders, who were masked to imaging modality and imaging timepoint. Graders were required to examine all SDOCT image series and record: (1) whether the imaging was acceptable, defined as the ability to see both the inner retinal surface and the retinal pigment epithelium (RPE) interface in at least one image, and (2) whether they could identify the following macular pathology or morphology on any scan captured in the series: (1) macular hole, (2) epiretinal membrane, (3) retinal edema, schisis, or cystoid structures, (4) subretinal fluid or retinal detachment, and (5) qualitative central retinal thickness from inner retina to RPE. Percent correlation between MIOCT and HHOCT at the same time-point for the detection of macular pathology was calculated by the number of features identified on MIOCT that were also identifiable on HHOCT.

Prior to initiation of human imaging, endpoints for satisfactory imaging were predefined as requirements to advance to subsequent study stages. These endpoints included (1) successful completion of surgery in all cases without interference from or serious adverse events related to the study, (2) acquisition of at least one acceptable image as defined above, and (3) greater than or equal to 80% MIOCT-to-HHOCT correlation of identification of the above listed pathology in greater than or equal to 80% of patients. Cohorts of five patients were imaged until all endpoints were achieved, and the study protocol allowed additional cohorts at the discretion of the imaging team. All patients were monitored postoperatively for adverse events.

Results

Stage 2 Intraoperative Imaging

Two sequential cohorts of five patients were imaged in Stage 2 of the MIOCT study, with intraoperative OCT imaging of patients first performed before macular surgery and then at an intraoperative pause in surgery (Table). The first cohort included eyes undergoing 25-gauge pars plana vitrectomy for removal of ERM ($n = 4$) and of VMT ($n = 1$). The second cohort consisted of 25-gauge pars plana vitrectomy for ERM ($n = 3$) and FTMH ($n = 2$). Through both cohorts, the MIOCT did not impair the surgeon's subjective ability to effectively perform

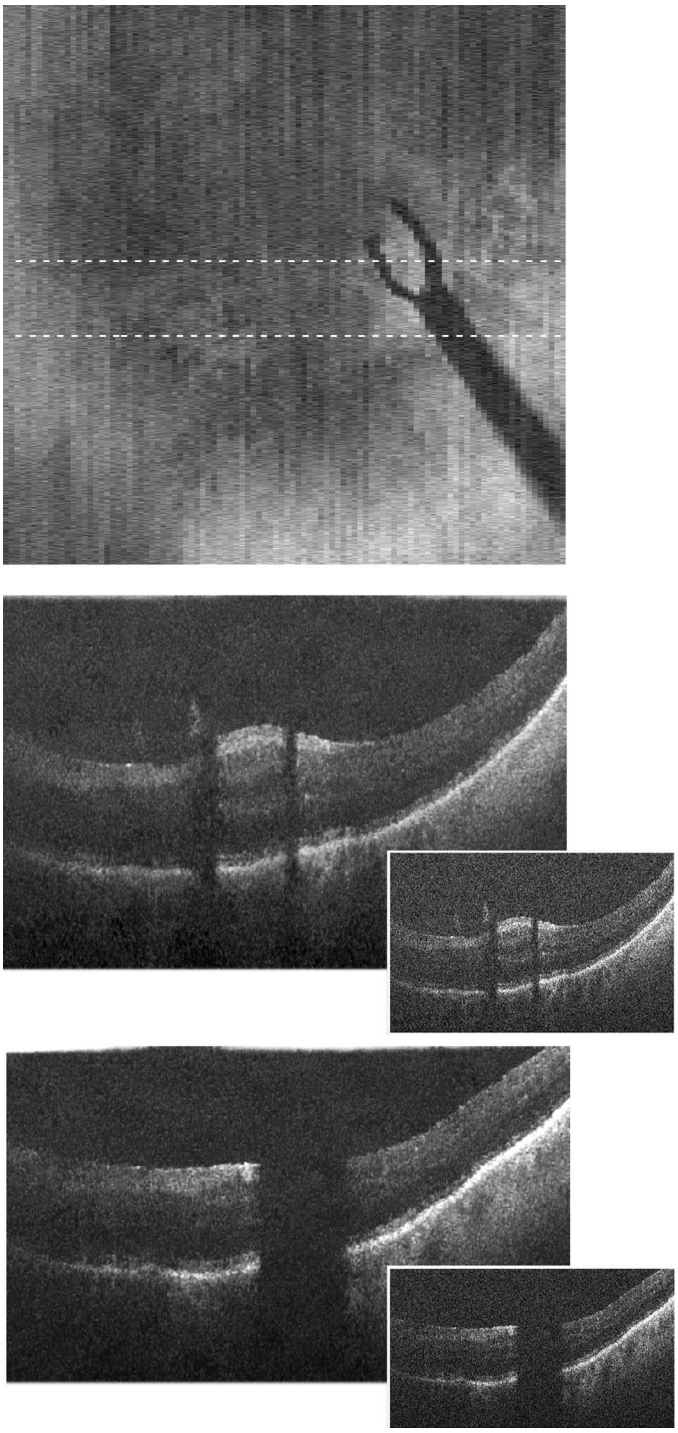

Figure 2. Retinal projection (*top*) of intraocular internal limiting membrane forceps overlying the retinal surface with *dashed white lines* designating the location of the extracted B-scans. Individual B-scan images (*middle and lower*) demonstrate complete shadowing under the metal instrument, with different shadowing patterns corresponding to different contours of the imaged instrument. The larger images were denoised with postprocessing algorithms; the *smaller insets* comprise the corresponding live, non-postprocessed images that were viewable by the research team intraoperatively in real time.

surgery in any surgical case, and there were no surgical complications or adverse events during any procedure or postoperatively. Imaging was graded as acceptable by predefined endpoints in all eyes.

Confirmation of preoperative diagnoses was achieved through review of Stage 2 MIOCT imaging in 90% of cases. MIOCT imaging confirmed successful completion of surgical goals (i.e., post peel absence of ERM overlying the fovea [Supplemental Fig. 1], absence of traction-inducing vitreous strands on the fovea, or removal of ILM as indicated by elevated perifoveal flaps) and confirmed the absence of iatrogenic complications (such as macular hole formation) in 80% of cases. In the remainder of cases, preoperative and intraoperative deficiencies were related to insufficient MIOCT image quality to adequately resolve an epiretinal membrane preoperatively in Case 4 and to adequately resolve presence or absence of an epiretinal membrane following peeling in Case 4 and 6 (Table).

Stage 2 imaging with instruments held static in the eye enabled, for the first time, MIOCT visualization of vitreoretinal instruments over the retinal surface. Imaging with metallic forceps in the midvitreous cavity resulted in complete shadowing of underlying retinal structures (Fig. 2). In contrast, imaging through the silicone tip of a diamond dusted membrane scraper allowed partial visibility of the underlying retina (Fig. 3). Objects positioned above the zero delay line resulted in a mirror image artifact that falsely suggests that the instruments are passing through the retinal surface (Fig. 3).

Comparison between MIOCT and HHOCT Stage 2 images demonstrated greater than or equal to 80% correlation in 80% of surgical cases (Table). Although the first cohort achieved its predefined endpoints, the imaging team made a voluntary decision to image a second cohort of five patients in order to gain more experience with MIOCT imaging prior to proceeding with Stage 3 imaging concurrent with surgical manipulations. In the second cohort, greater than or equal to 80% correlation between MIOCT and HHOCT was similarly achieved in 80% of cases. Image analysis was performed with unprocessed single OCT B-scan images. Although image processing was helpful in denoising the images, unprocessed image quality was sufficiently high that postprocessing did not reveal any previously unidentified pathology.

Stage 3 Imaging

Following successful completion of Stage 2 imaging in two separate cohorts, Stage 3 imaging was initiated,

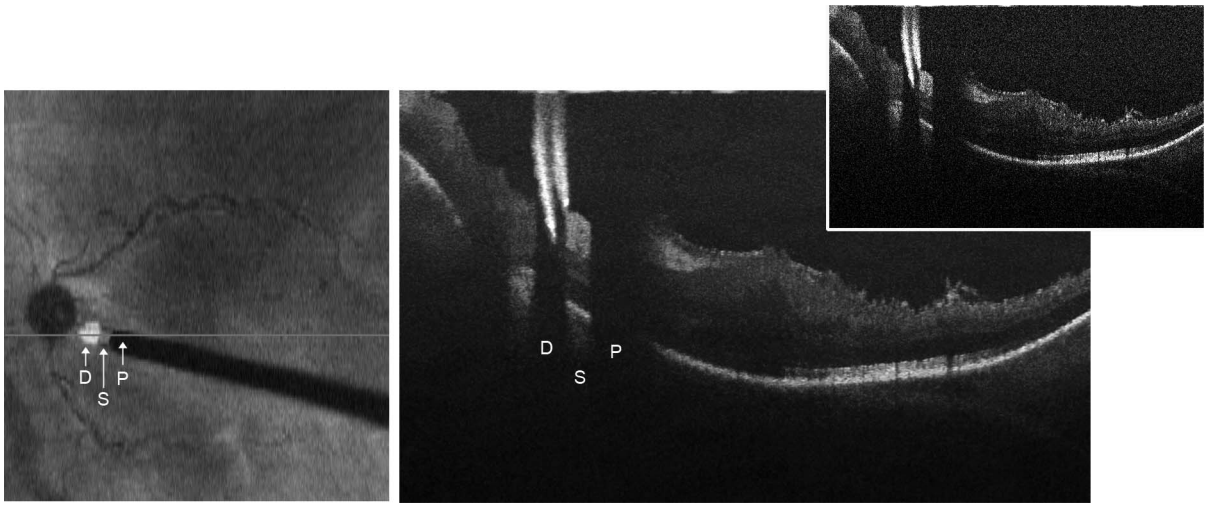

Figure 3. Retinal projection (*left*) of a diamond dusted membrane scraper overlying the retinal surface and an individual B-scan (*right*) demonstrating the instrument overlying the retina with complete shadowing through the diamond-dusted tip (D) and the dense metal shaft (P) but near total visibility through the bare silicone portion of the instrument tip (S). An epiretinal membrane is clearly identified on the B-scan image, which was obtained prior to membrane peeling. The tip of the instrument appears to extend into the retina; however, this is a mirror image artifact caused by the instrument's position, which is above the zero delay line of the SDOCT and also well above the retinal surface. The larger image was denoised with postprocessing algorithms; the *smaller inset* comprises the corresponding live, non-postprocessed image that was viewable by the research team intraoperatively in real-time.

enabling MIOCT acquisition simultaneous with dynamic surgical manipulations to visualize instrument-retina interaction. Early in Stage 3, the difficulty of such acquisition was realized. Because of the movement of the surgical instrument into and out of the MIOCT imaging field without a means to independently adjust the position of the MIOCT beam in real-time and/or obtain multiple scans spanning a macular volume in real-time, only maneuvers occurring within the fixed region of OCT acquisition could be imaged. To address this difficulty, an OCT tracking system was developed to allow live, dynamic targeting of the OCT beam in real-time to any area of interest (see Methods). Acquisition of sequential B-scans, when appropriately targeted to the location of a continually moving instrument, provided cross-sectional images of instrument interactions with the retina in real time for the first time using this prototype device in surgery (Fig. 4, Supplemental Video 1).

Discussion

In this study, we present intraoperative imaging results obtained during Stage 2 and 3 of a prospective translational study designed to characterize MIOCT imaging during vitreoretinal surgery with instruments in the eye. All surgical procedures using this prototype device were successfully performed without complication or adverse events, and in all cases, the surgeon did not feel that the MIOCT unit interfered with surgery. Live images without any postprocessing modifications maintained high resolution and were graded acceptable (versus not acceptable), as defined by predetermined criteria in all cases (Figs. 2–4). While postprocessing denoising algorithms were useful in improving the signal-to-noise ratio for publication purposes, these post-processed images did not reveal any new pathology not identified in the live, unprocessed images.

We previously reported results from Stage 1 of intraoperative MIOCT imaging, obtained without instruments in the eye, in which a learning curve to properly orient the eye and obtain images through the fovea resulted in failure to achieve predefined endpoints in the first cohort imaged.[1] During Stage 2 of MIOCT intraoperative imaging, orientation of MIOCT was performed through manipulation of instruments in the vitreous cavity to optimize the surgeon's view through the surgical microscope, resulting in orientation and imaging that were significantly more intuitive to a surgeon than without instruments in the eye. Successful Stage 2 MIOCT imaging and acceptable correlation with HHOCT imaging, which was the only means, and thus standard of intraoperative imaging at the time of study design,

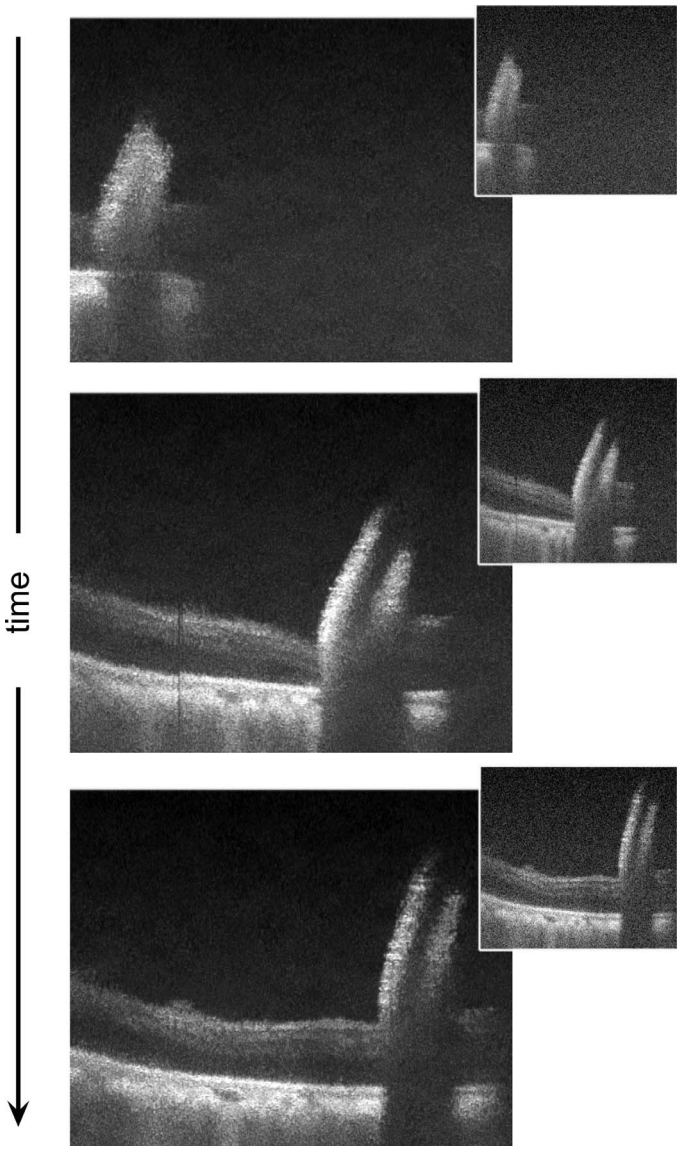

Figure 4. Single MIOCT B-scan frames from real-time video imaging (see Supplemental Video 1) targeted using a dynamic OCT tracking system to the longitudinal axis of the diamond-dusted membrane scraper brushing against the retinal surface during epiretinal membrane removal. The larger images were denoised with post-processing algorithms; the *smaller insets* comprise the corresponding live, non-postprocessed images that were viewable by the research team intraoperatively in real-time.

was obtained in both cohorts of five patients, demonstrating the ability of the MIOCT device to acquire images with clinically relevant details.

Similar to our previous report with Stage 1 MIOCT imaging,[1] Stage 2 images reported herein were able to confirm preoperative pathology and identify postsurgical changes in retinal morphology, including successful completion of surgical goals such as ERM removal (Supplemental Fig. 1), VMT relief, and ILM peeling. Completion of surgical goals and absence of iatrogenic complications was confirmed with MIOCT imaging in all eyes in which intraoperative images were of adequate quality to qualitatively visualize retinal morphology details (80% of eyes). Quantitative assessments of these changes require calibration of our MIOCT device according to novel algorithms that would account for changes in refractive indices induced the by BIOM and flat lens. While these algorithms were not available at the time of this study, quantitative analysis of intraoperative changes will be a goal of future investigations.

A recent prospective study of handheld OCT imaging obtained at pauses in surgery has demonstrated the importance of intraoperative OCT in surgical decision making.[22] This impact not yet been systematically assessed with our or other microscope-integrated OCT systems that have been recently developed (iOCT; Haag-Streit, Wedel, Germany and RESCAN 700; Carl Zeiss Meditec, Oberkochen, Germany[16,17]). These commercial systems are not currently available in the United States, and these systems have not been formally compared with HHOCT imaging. As we have demonstrated in this and a previous report,[1] MIOCT imaging at pauses in surgery provides comparable images to HHOCT systems, and it is likely that MIOCT imaging therefore maintains this benefit of enhanced surgical decision making.

The true benefit of MIOCT imaging is the ability to acquire images not at full pauses in surgery but with instruments in the eye and especially concurrent with surgical manipulations. For the first time in humans using this device, we were able to use OCT to visualize instruments within the vitreous cavity, including intraocular forceps (Alcon, Fort Worth, TX) and the diamond dusted membrane scraper (Synergetics, O'Fallon, MO). As we and others have previously reported in model eyes, metallic instruments result in complete shadowing of underlying structures, whereas silicone instrumentation, such as the tip of the Tano scraper, allows partial transmission and therefore visualization of underlying retinal structures.[12,14,19,23] While visualization under the instrument is currently limited and does not assist in performing surgical maneuvers at this time, its identification highlights the potential use of instrument development with novel materials optimized for OCT visualization of underlying retinal structures.[12]

During MIOCT imaging with instruments in the eye, we identified significant technological deficiencies

preventing seamless real-time MIOCT imaging of surgical manipulations. First, mirror-image artifacts caused by instruments extending above the zero delay line falsely suggest that these instruments are passing through the retinal surface. We have previously reported on use of an inverted imaging technique, similar to enhanced depth imaging employed by the Heidelberg Spectralis SDOCT system (Heidelberg Engineering, Inc., Carlsbad, CA),[24] to shift the zero delay position below the retina, rather than above, as is normally performed for retinal imaging.[14] We are currently exploring this technique for MIOCT imaging in human eyes. Hardware and software modifications to increase the axial imaging range would also minimize these artifacts. In particular, we are currently developing a next-generation MIOCT system employing swept-source OCT technology, which in addition to featuring faster imaging speed, enables longer scan depth and the potential for complete removal of the mirror image artifact.

The most important deficiency we identified was the absence of a targeting system to direct the OCT to an area of interest. A targeting system was not important for Stage 1 or Stage 2, which obtained imaging at a static time point. Stage 3 imaging, performed concurrent with active surgical manipulations and with a goal of viewing the site of instrument-tissue interaction, required dynamic relocation of the area of OCT imaging. Such dynamic imaging could only be obtained with real-time volume acquisition and/or the ability to continually target the OCT beam in real-time. We have recently developed such a tracking system. While this system is currently controlled by a technician manually targeting the desired imaging location intraoperatively by moving a mouse cursor over the surgical video feed, we are currently developing automated and surgeon-controlled tracking systems to follow a moving instrument or target. We predict that MIOCT image tracking will significantly improve our ability to obtain intrasurgical images of dynamic changes in retinal morphology in real time. We are also developing and testing a swept-source OCT based MIOCT system, whose increased speed will allow for near real-time volumetric retinal imaging for the first time. Near real-time volumetric imaging should relax the constraint for constant tracking of the OCT imaging location to the precise location of the surgical tool and should lead to even more seamless surgical integration and understanding of the impact of MIOCT on surgical approach and decision-making.

Acknowledgments

The authors thank Fernando Tineo for his assistance with the illustration.

Supported by the National Institutes of Health Grant 1R01EY023039 and R21 EY019411.

Disclosures: **P. Hahn,** consulting agreement unrelated to the submitted work with Second Sight Medical Products, Inc; **O. Carrasco-Zevallos,** None; **D. Cunefare,** None; **J. Migacz,** None; **S. Farsiu,** research support through his university from the National Eye Institute/National Institutes of Health and patents pending in OCT imaging and analysis; **J.A. Izatt,** royalties through his university from licensed patents in OCT technology, co-founder and Chief Scientific Officer at Bioptigen, Inc. with corporate, equity, and intellectual property interests; **C.A. Toth,** research support through her university from the National Eye Institute/National Institutes of Health, Bioptigen, and Genentech, and royalties through her university from Alcon and patents and patents pending in OCT imaging and analysis

References

1. Hahn P, Migacz J, O'Donnell R, et al. Preclinical evaluation and intraoperative human retinal imaging with a high-resolution microscope-integrated spectral domain optical coherence tomography device. *Retina*. 2013;33:1328–1337.
2. Dayani PN, Maldonado R, Farsiu S, Toth CA. Intraoperative use of handheld spectral domain optical coherence tomography imaging in macular surgery. *Retina*. 2009;29:1457–1468.
3. Lee LB, Srivastava SK. Intraoperative spectral-domain optical coherence tomography during complex retinal detachment repair. *Ophthalmic Surg Lasers Imaging*. 2011;42:e71–e74.
4. Ray R, Baranano DE, Fortun JA, et al. Intraoperative microscope-mounted spectral domain optical coherence tomography for evaluation of retinal anatomy during macular surgery. *Ophthalmology*. 2011;118:2212–2217.
5. Wykoff CC, Berrocal AM, Schefler AC, Uhlhorn SR, Ruggeri M, Hess D. Intraoperative OCT of a full-thickness macular hole before and after internal limiting membrane peeling. *Ophthalmic Surg Lasers Imaging*. 2010;41:7–11.

6. Scott AW, Farsiu S, Enyedi LB, Wallace DK, Toth CA. Imaging the infant retina with a hand-held spectral-domain optical coherence tomography device. *Am J Ophthalmol*. 2009;147:364–373.
7. Ehlers JP, Kernstine K, Farsiu S, Sarin N, Maldonado R, Toth CA. Analysis of pars plana vitrectomy for optic pit-related maculopathy with intraoperative optical coherence tomography: a possible connection with the vitreous cavity. *Arch Ophthalmol*. 2011;129:1483–1486.
8. Ehlers JP, Ohr MP, Kaiser PK, Srivastava SK. Novel microarchitectural dynamics in rhegmatogenous retinal detachments identified with intraoperative optical coherence tomography. *Retina*. 2013;33:1428–1434.
9. Pichi F, Alkabes M, Nucci P, Ciardella AP. Intraoperative SD-OCT in macular surgery. *Ophthalmic Surg Lasers Imaging*. 2012;43:S54–S60.
10. Ehlers JP, Xu D, Kaiser PK, Singh RP, Srivastava SK. Intrasurgical dynamics of macular hole surgery: an assessment of surgery-induced ultrastructural alterations with intraoperative optical coherence tomography. *Retina*. 2014;34:213–221.
11. Tao YK, Ehlers JP, Toth CA, Izatt JA. Intraoperative spectral domain optical coherence tomography for vitreoretinal surgery. *Opt Lett*. 2010;35:3315–3317.
12. Ehlers JP, Tao YK, Farsiu S, Maldonado R, Izatt JA, Toth CA. Integration of a spectral domain optical coherence tomography system into a surgical microscope for intraoperative imaging. *Invest Ophthalmol Vis Sci*. 2011;52:3153–3159.
13. Ehlers JP, Tao YK, Farsiu S, Maldonado R, Izatt JA, Toth CA. Visualization of real-time intraoperative maneuvers with a microscope-mounted spectral domain optical coherence tomography system. *Retina*. 2013;33:232–236.
14. Hahn P, Migacz J, O'Connell R, Izatt JA, Toth CA. Unprocessed real-time imaging of vitreoretinal surgical maneuvers using a microscope-integrated spectral-domain optical coherence tomography system. *Graefes Arch Clin Exp Ophthalmol*. 2013;251:213–220.
15. Huttmann G, Lankenau E, Schulz-Wackerbarth C, Muller M, Steven P, Birngruber R. Optical coherence tomography: from retina imaging to intraoperative use - a review. *Klin Monbl Augenheilkd*. 2009;226:958–964.
16. Binder S, Falkner-Radler CI, Hauger C, Matz H, Glittenberg C. Feasibility of intrasurgical spectral-domain optical coherence tomography. *Retina*. 2011;31:1332–1336.
17. Ehlers JP, Kaiser PK, Srivastava SK. Intraoperative optical coherence tomography using the RESCAN 700: preliminary results from the DISCOVER study. *Br J Ophthalmol*. 2014;98:1329–1332.
18. Tao YK, Ehlers JP, Toth CA, Izatt JA. Visualization of vitreoretinal surgical manipulations using intraoperative spectral domain optical coherence tomography. *Proc SPIE*. 2011;7889:78890F.
19. Hahn P, Migacz J, O'Connell R, Maldonado R, Izatt JA, Toth CA. The use of optical coherence tomography in intraoperative ophthalmic imaging. *Ophthalmic Surg Lasers Imaging*. 2011;42:S85–S94.
20. Fang L, Li S, McNabb RP, et al. Fast acquisition and reconstruction of optical coherence tomography images via sparse representation. *IEEE Trans Med Imaging*. 2013;32:2034–2049.
21. Srinivasan PP, Heflin SJ, Izatt JA, Arshavsky VY, Farsiu S. Automatic segmentation of up to ten layer boundaries in SD-OCT images of the mouse retina with and without missing layers due to pathology. *Biomed Opt Express*. 2014;5:348–365.
22. Ehlers JP, Dupps WJ, Kaiser PK, et al. The Prospective Intraoperative and Perioperative Ophthalmic ImagiNg with Optical CoherEncE TomogRaphy (PIONEER) Study: 2-year Results. *Am J Ophthalmol*. 2014;158:999–1007.
23. Ehlers JP, Srivastava SK, Feiler D, Noonan AI, Rollins AM, Tao YK. Integrative advances for OCT-guided ophthalmic surgery and intraoperative OCT: microscope integration, surgical instrumentation, and heads-up display surgeon feedback. *PLoS ONE*. 2014;9:e105224.
24. Spaide RF, Koizumi H, Pozzoni MC. Enhanced depth imaging spectral-domain optical coherence tomography. *Am J Ophthalmol*. 2008;146:496–500.